Hydrodynamic Performance Analysis of Large-Amplitude Undulating Fin Propulsion

Rui Zhu*, Zhi-Dong Wang and Guohuai Sun

School of Naval Architecture and Ocean Engineering, Jiangsu University of Science and Technology, Zhenjiang, Jiangsu, 212100, China
*Corresponding author's e-mail: zhurui8371113@163.com

Abstract. Apteronotus albifrons possesses an elongated anal fin that enhances its cruising efficiency and maneuverability in complex environments. This study utilizes a three-dimensional numerical model in conjunction with dynamic mesh technology to analyze the hydrodynamic properties of a large-amplitude undulating fin under varying flow velocities and oscillation amplitudes. Based on the "differential first, then integral" approach, the thrust coefficient and propulsion efficiency of the undulating fin are evaluated using computational simulation methods. The results indicate that as the advance ratio increases, the thrust coefficient gradually decreases, becoming negative when the advance ratio reaches 1. At an advance ratio of 0.75, the average propulsion efficiency peaks at approximately 65.8%. Furthermore, larger oscillation amplitudes contribute to an increase in the thrust generated by the undulating fin, significantly enhancing its overall operational performance. These findings provide essential methodologies and theoretical support for the future optimization and design of undulating fins.

Keywords: Large-Amplitude Undulating Fin; Propulsive efficiency; Numerical simulation; Hydrodynamic performance

1 Introduction

Through long-term natural selection and evolution, fish have developed efficient propulsion systems and exceptional maneuverability in water. In recent years, biomimetic propulsion technology has emerged as a key focus in underwater vehicle research, attracting significant attention [1]. The remarkable swimming abilities of fish have fueled advancements in biomimetic research, which categorize fish propulsion into two primary methods: body and/or caudal fin (BCF) propulsion and median and/or paired fin (MPF) propulsion. BCF propulsion, utilized by most fish, enables high-speed cruising and rapid acceleration, although it tends to be less efficient and generates more turbulence. In contrast, the MPF propulsion mode provides improved maneuverability and efficiency in complex underwater environments. Undulating fin propulsion is regarded as having significant potential for the design of new uncrewed underwater robotics.

Numerous scholars, both domestically and internationally, have extensively studied oscillating fin propulsion systems, focusing on their configurations, hydrodynamic properties, and propulsion mechanisms. In 2005, Epstein et al. [2] investigated the propulsion performance of the weakly electric knifefish (Apteronotus albifrons, Figure 1) using computational fluid dynamics (CFD). They explored the relationships between thrust and parameters such as frequency, amplitude, and wavelength, revealing the impact of vortices on efficiency.

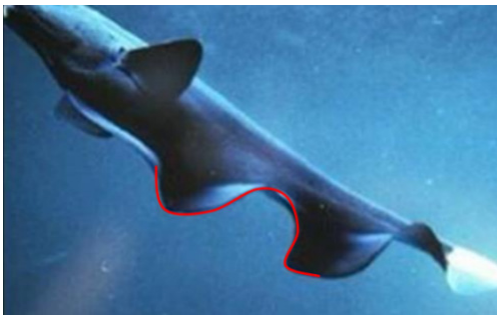

Fig. 1. Photo of Apteronotus albifrons.

In 2007, Wang et al. [3] conducted both theoretical and experimental studies on long dorsal fin undulating propulsion, examining the oscillatory mechanism, propulsion efficiency, and flow field characteristics. The maximum amplitude of the fin rays reached 30°. Rahman et al. (2010) performed numerical simulations on dual undulating fins to investigate the mechanisms of thrust generation. Their findings indicated that thrust and propulsion efficiency are primarily influenced by the aspect ratio and fin angle.

Hu et al. [4] focused on analyzing the hydrodynamic performance of undulating fin propulsion systems. Through computational fluid dynamics (CFD) simulations and experiments, they investigated how parameters like undulation frequency, amplitude, and speed affect thrust and efficiency. In 2020, Liu et al. [5] designed an undulating fin robot that mimics aquatic swimming patterns. Computational fluid dynamics (CFD) simulations and tests demonstrated excellent maneuverability and efficiency; however, the robot exhibited a limitation in speed.

In 2023, Zhang et al. [6] studied the hydrodynamics of undulating fins using the knifefish as a biomimetic model. Through simulations and experiments, they analyzed thrust, efficiency, and fluid dynamics, providing insights for optimizing bio-inspired propulsion. The maximum amplitude of the fin rays was 30°.

In the studies mentioned above, the amplitude of the undulating fins typically does not exceed 45°, and there is relatively limited research on large-amplitude torsional wave propulsion fins. Large-amplitude movements can significantly influence hydrodynamic characteristics, particularly thrust, propulsion efficiency, and flow field properties. Existing studies provide limited insight into how large-amplitude fin movements affect hydrodynamic performance, particularly in terms of thrust and efficiency, with minimal emphasis on the balance between amplitude and propulsion.

Consequently, this paper utilizes the knifefish (Apteronotus albifrons) as a model organism, designing undulating fins with a 65° amplitude and high fidelity. The study examines their hydrodynamic performance across a range of flow velocities and oscillation amplitudes. By employing a "differentiation followed by integration" method to calculate propulsion efficiency, the research enhances the accuracy of assessments, enabling a more precise evaluation of large amplitude undulating fins. This study provides valuable insights for optimizing biomimetic propulsion systems and lays the groundwork for developing more efficient and flexible underwater robots and unmanned underwater vehicles (UUVs).

The structure of this study is outlined as follows: Section 2 discusses motion control equations for large-amplitude undulating fins and outlines the numerical methods employed for the calculations, utilizing a "differentiation followed by integration" approach to enhance the accuracy of propulsion efficiency. In Section 3, the effects of various flow velocities and oscillation amplitudes on propulsion performance are examined, along with an exploration of changes in vorticity contours for the undulating fins. Finally, Section 4 summarizes the key findings and conclusions of the study.

2 Problem Description

2.1 The Equation of Motion for Undulating Fin

The dynamics of biomimetic fish fins are modeled using a fundamental frequency simple harmonic wave, with each fin ray oscillating like a simple harmonic pendulum about the X-axis. By controlling the variation in the oscillation angle along the X-axis, the overall movement pattern of the fin is regulated. Figure 2 illustrates both the three-dimensional view and the side view of the large-amplitude undulating fin.

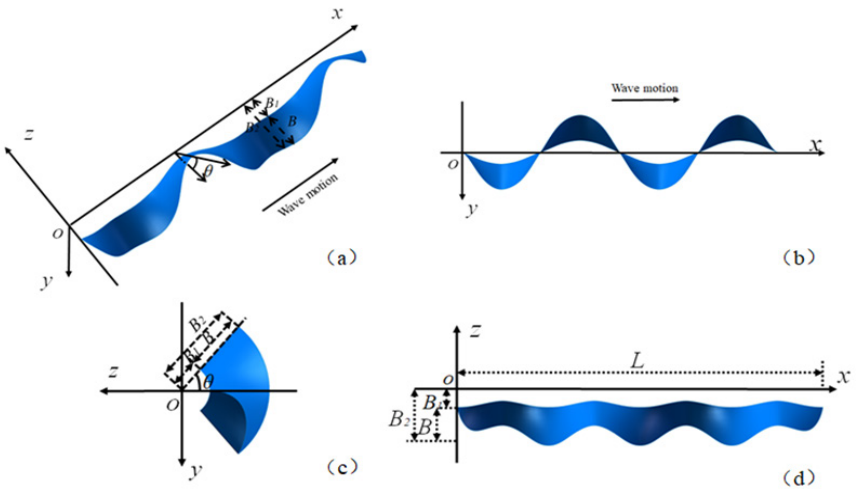

Fig. 2. Wave fin schematic diagram. (a) 3D view, (b) bottom view, (c) front view, (d) side view.

This study examines the hydrodynamic performance of a large-amplitude undulating fin while excluding the effects of fluid-structure interaction. The computational model employed has a thickness of 0 mm, a length of 1380 mm, and a width of 150 mm. The parametric equation of the fin surface in Cartesian coordinates is expressed as:

$$\begin{cases} p_x(r,l,t) = l \\ p_y(r,l,t) = r \cdot \cos(\theta(l,t)) \\ p_z(r,l,t) = r \cdot \sin(\theta(l,t)) \\ 0 < r < B, 0 < l < L \end{cases} \tag{1}$$

In the equation, r represents the variation along the length of the fin ray, with a maximum value of B; l denotes the variation along the baseline of the fin surface, with a maximum value of L; t is the time variable. The angular variation of the fin ray at position l can be described by the following sine curve:

$$\theta(l,t) = \theta_{\max} \cdot \sin(\frac{2\pi}{T}t - \frac{2\pi}{\lambda}l + \phi_0) \tag{2}$$

where θ_{max} is used to describe the maximum swing angle of the fin, f denotes the oscillation frequency, T represents the period, λ indicates the wavelength, and Φ_0 is the initial displacement of the first fin ray, signifying the initial stage of the fin's undulating motion. The initial phases of all fin rays follow an arithmetic sequence.

2.2 Numerical Method

The undulating fin in this study is used in the propulsion system of an amphibious robot and features higher stiffness for land movement. With minimal fluid impact, the simulations focus solely on torsional wave propulsion, excluding fluid-structure interaction. Instead, the commercial computational fluid dynamics (CFD) solver Fluent, along with custom user-defined functions (UDFs), is utilized to ensure accurate modeling of fin dynamics and flow behavior. For a viscous three-dimensional incompressible fluid, this study employs the Reynolds-Averaged Navier-Stokes (RANS) equations for calculations [7]. The continuity and momentum equations are expressed as follows:

$$\rho \frac{\partial u_i}{\partial x_i} = 0 \tag{3}$$

$$\rho \frac{\partial u_i}{\partial t} + \rho \frac{\partial (u_i u_j)}{\partial x_j} = -\frac{\partial p}{\partial x_i} + \frac{\partial}{\partial x_j}(\mu \frac{\partial u_i}{\partial x_j} - \rho \overline{\mu_i' \mu_j'}) + S_i \tag{4}$$

In the equations, ρ represents fluid density, μ_i is the average velocity component, P is the average pressure, μ denotes the dynamic viscosity, $\rho\overline{\mu_i'\mu_j'}$ is the Reynolds stress term that accounts for turbulence effects, and S_i is the volume force.

The Reynolds number calculated from L and U_0 is Re = 1.6×10^6, t, assuming turbulent flow over the fin surface. The *SST k-ω* [8] model is adopted for its ability to accurately capture shear stress and effectively control pressure gradients near the wall. For incompressible fluids, spatial discretization is performed using the finite volume method, with a second-order upwind scheme employed to enhance accuracy. A segregated solution approach is applied to the discrete equations, with the SIMPLE [9] algorithm implemented for simulations involving small time steps. Time discretization employs an implicit first-order scheme with a time step of 0.001 seconds over five wave periods.

2.3 Calculation Method for Propulsion Efficiency of Undulating Fin

The advance ratio, derived from propeller theory, represents the speed at which a propeller moves along its axis in relation to the water. In this study, it is defined as the propagation speed of the traveling wave on the undulating fin.

$$J = \frac{U}{f \cdot \lambda} \tag{5}$$

The non-dimensional thrust coefficient is defined as follows [4]:

$$C_T = \frac{T}{\rho \cdot f^2 \cdot B^2 \cdot L^2} \tag{6}$$

where T represents the thrust generated during the propulsion of the long fin with torsional oscillation, f denotes the oscillation frequency of the fin, B represents the height of the fin, L represents the length of the fin, and ρ represents the density of water.

In the field of robotics, efficiency is precisely defined as the ratio of output power to input power. Several parameters are used to describe the hydrodynamic performance of an undulating fin: thrust (T_x), output power (P_x), input power (P), and propulsion efficiency (η). For a single propeller, the input power (P) is calculated as the product of motor torque (M) and angular velocity (Ω). Meanwhile, the effective output power (P_{out}) is determined by multiplying the measured thrust (T) by the flow velocity (U). The propulsion efficiency is defined as follows:

$$\eta = \frac{P_{out}}{P} = \frac{TU}{M\Omega} \tag{7}$$

In the equation, the thrust T corresponds to the undulating fin's thrust T_x and the flow velocity U matches the incoming flow velocity U_0 in numerical calculations.

Due to the periodic changes in angular velocity and torque over time at various positions across the entire undulating fin, the average torque ultimately equals zero. This study employs a followed-by-integration approach to calculate propulsion efficiency, dividing the undulating fin into several differential cells, as illustrated in Figure 3.

The undulating fin is segmented into three sections, comprising a total of 30 differential cells. The head and tail of the oscillating fin are more sensitive to the influences of incoming and outgoing water flows, the width of the head and tail regions is set to n_1=0.044 m, while the width of the central portion is n_2=0.05 m. The final propulsion efficiency is calculated as follows [10]:

$$\eta = \frac{P_x(t)}{P(t)} = \frac{\int_0^L T_x(l,t)U_0 dl}{\int_0^L M_x(l,t)\Omega(l,t)dl} \tag{8}$$

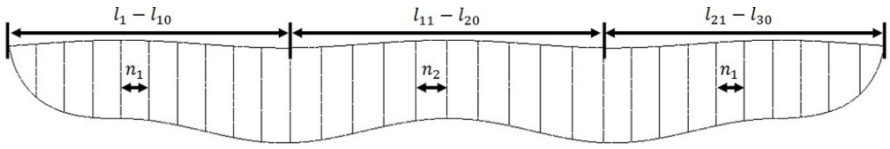

Fig. 3. Schematic diagram of differential unit division.

2.4 Computational Domain, Boundary Conditions, and Mesh Generation

In the numerical simulation of large-amplitude undulating fins, two key challenges emerge. First, the propulsion mechanism of these fins involves complex fluid dynamics. The periodic and large-amplitude undulating motions cause the fin surface to undergo intricate deformations continuously. This necessitates constant adjustments to the shape and position of the computational grid near the fin. Therefore, dynamic mesh technology is required to update the grid at the moving boundaries and precisely capture the vortex structures caused by the motion of the fin. Second, precise motion equations must be established using User-Defined Functions (UDFs) to control the motion of the undulating fin. Addressing these two factors is critical for ensuring accurate simulations and optimizing the hydrodynamic performance of large-amplitude undulating fin.

Therefore, a hybrid mesh division is employed in the computational domain. Figure 4 illustrates this division. The dimensions of the outer computational domain are 3.5L × L × L, while the inner domain measures 2L × 0.5L × 0.5L, where L represents the fin length (1380 mm). The velocity inlet is located along the negative X-axis, and the pressure outlet is located behind the trailing edge, at a distance twice the length of the fin. The upper, lower, left, and right boundaries serve as symmetry planes.

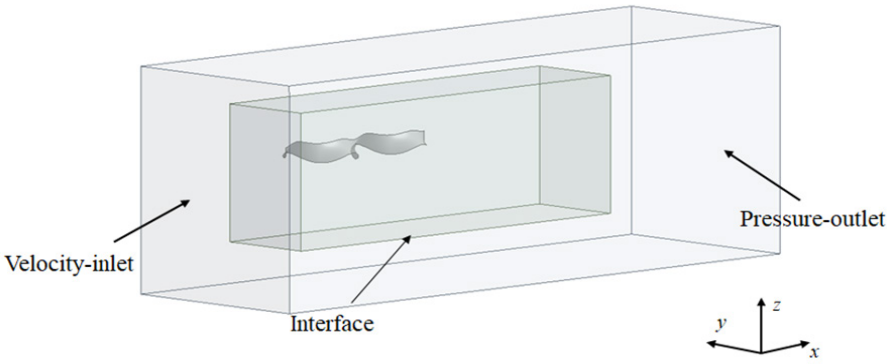

Fig. 4. Division of the computational domain.

Due to the large amplitude motion of the undulating fin, significant mesh deformations occur. To prevent the formation of negative-volume cells, the dynamic grid is updated using a diffusion smoothing technique and a local mesh reconstruction method. Local mesh refinement is applied around the fin, while coarser mesh sizes are utilized in other fluid regions. Data is transferred between the outer and inner domains through an interface, with the mesh size gradually expanding from this interface. The fin surface mesh is generated separately, resulting in a total of 2.82 million mesh elements. The maximum skewness is below 0.69, indicating good orthogonality. Figure 5 illustrates the results of the mesh generation.

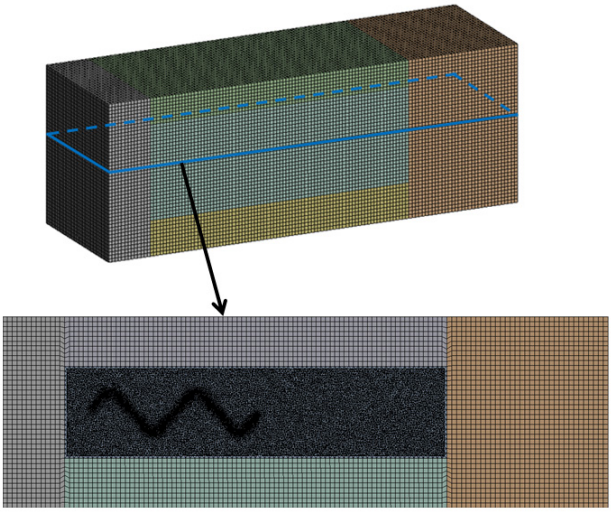

Fig. 5. Hydrodynamic computational mesh for large-amplitude oscillating flexible long-fin propulsion.

2.5 Grid Independence Verification

To guarantee that the quantity of mesh elements satisfies the accuracy requirements for numerical simulations, mesh convergence verification is essential. The following parameters are selected as the basic conditions for the numerical calculation of the undulating fin: L = 1.38 m, B = 0.15 m, inflow velocity U_0 = 0.5 kn, maximum amplitude A = 50°, wavelength λ = 0.69 m, and oscillation frequency f = 1 Hz. Five mesh configurations with varying element counts are generated for convergence verification: 0.89 million, 1.25 million, 1.77 million, 2.78 million, and 3.56 million. The instantaneous thrust is calculated over multiple cycles for mesh configuration, and the average thrust within a single cycle is determined. The results are shown in the Table 1 below.

Table 1. Average Thrust of an Undulating Fin over a Single Cycle at Varying Grid Resolutions.

Number of Grid (×10⁴)	89 W	125 W	177 W	278 W	353 W
T_x (N)	12.9733	12.9978	13.1063	13.1074	13.1079

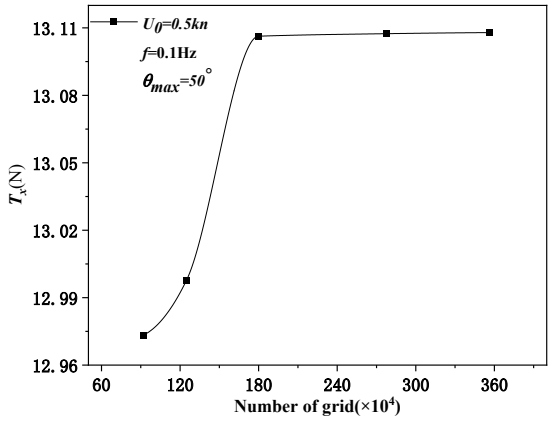

Fig. 6. Mesh convergence verification.

As illustrated in Figure 6, the calculated average thrust approaches 13.1 N as the number of mesh elements increases, achieving a relative error of less than 0.01%. This result indicates convergence at 2.78 million elements. Taking into account memory usage, computation time, and numerical accuracy, the mesh comprising 2.78 million elements is selected for the numerical simulation of the hydrodynamic performance of the large amplitude undulating fin.

3 Hydrodynamic Calculation Results and Analysis

The control variable method is utilized for a hydrodynamic numerical study of the primary parameters of undulating fins. To effectively illustrate the general motion

patterns, typical working conditions are established: an inflow velocity of 0.5 knots, a wavelength-to-fin-length ratio of 1, a maximum oscillation angle of 50°, and an oscillation frequency of 1.00 Hz. Once the computed thrust, lateral force, lift, and input power achieve periodic convergence, the average values over multiple cycles are calculated as single-cycle averages and non-dimensionalized using dimensionless numbers.

3.1 Influence of Inflow Velocity

With a wavelength-to-fin-length ratio of λ/L = 0.5, an oscillation amplitude angle of θ_{max} = 50°, and an oscillation frequency of f = 1 Hz, the advance ratio J is determined exclusively by the inflow velocity U_0.

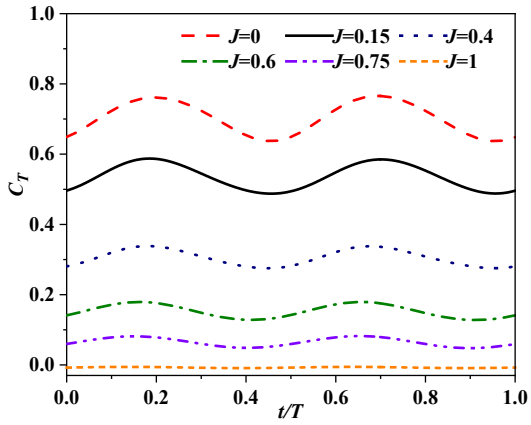

Fig. 7. Thrust coefficient variation curve over one cycle at different advance ratios.

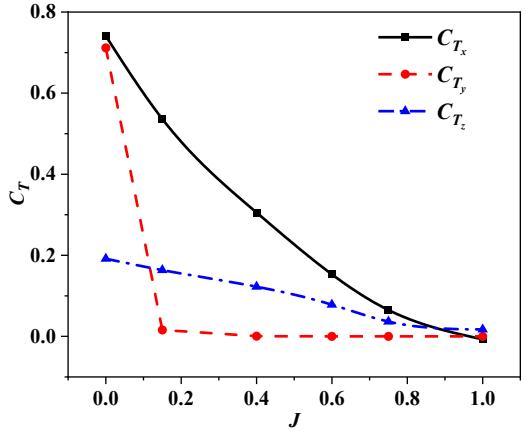

Fig. 8. Force coefficient curves at varying advance ratios.

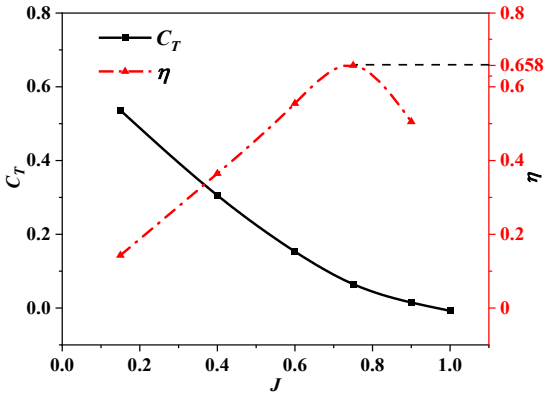

Fig. 9. The variation curves of propulsive efficiency under different advance ratios.

Figure 7 illustrates that the thrust coefficient varies twice within a single cycle for different advance ratios, exhibiting a "W" shape. With an increase in the advance ratio, the thrust coefficient decreases, ultimately becoming negative at an advance ratio of 1.

Figure 8 illustrates the variation curves of average thrust, lateral force, and lift coefficients across different advance ratios. With an increase in the advance ratio, the thrust, lateral force, and lift coefficients gradually decrease and stabilize. Notably, when the advance ratio is below 0.8, the average thrust coefficient consistently surpasses both the lateral force and lift coefficients. Figure 9 indicates that the undulating fin attains its maximum propulsion efficiency of 65.8% at an advance ratio of 0.8.

This paper employs the Q criterion to evaluate vortex intensity around the undulating fin. Figure 10 illustrates the vorticity curves of the fins at various advance ratios on the z = -0.14 m plane.

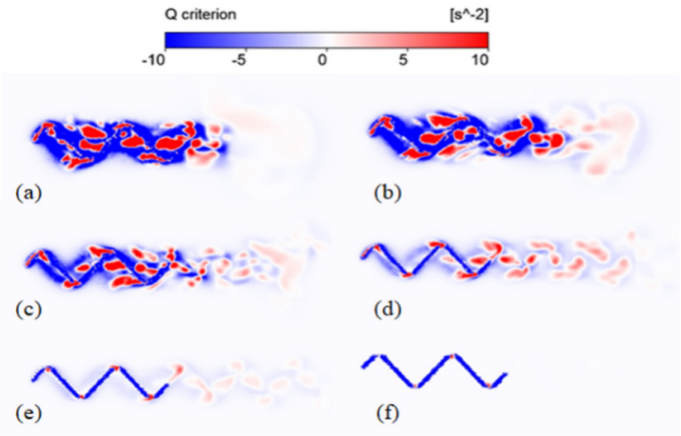

Fig. 10. Vorticity contours of the undulatory fin at different advance ratios: (a) J=0, (b) J=0.15, (c) J=0.4, (d) J=0.6, (e) J=0.75, (f) J=0.1.

When the advance ratio is low, the vortex distribution is dense and robust. With an increase in the advance ratio, the formation of vortices at the fin's leading edge becomes increasingly challenging, while the dissipation rate at the trailing edge accelerates. This leads to a gradual decrease in both the number and strength of the vortices. These findings indicate that a higher incoming flow velocity directly influences the vortex structure and improves the hydrodynamic performance of the undulating fin.

3.2 Influence of Amplitude

When the fin height is fixed, varying the oscillation angle affects the amplitude of the undulating fin. Numerical calculations produce a curve that illustrates the variation of the thrust coefficient over a single cycle at various oscillation angles, as shown in Figure 11.

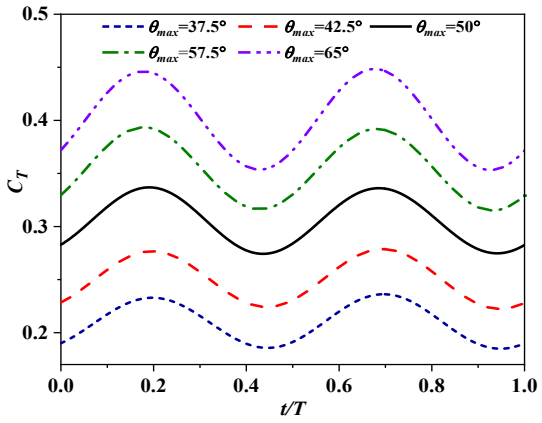

Fig. 11. Thrust coefficient variation within a single cycle at different oscillation angles.

The variation of the thrust coefficient at different oscillation angles displays a periodic pattern akin to that observed at various advanced ratios. As the oscillation amplitude increases, the thrust coefficient steadily rises, and its fluctuations become more pronounced. Notably, when the maximum angle reaches 65°, the fluctuation period exhibits significant changes compared to smaller amplitudes.

Figure 12 illustrates the curves representing the average thrust, lateral force, and lift coefficients of the undulating fin at different oscillation amplitudes. It is clear that thrust increases significantly with larger oscillation amplitudes, while the lift and lateral force remain relatively constant.

Moreover, as illustrated in Figure 13, the hydrodynamic characteristics demonstrate that the propulsion efficiency of the undulating fin remains relatively constant at approximately 36.5% as the oscillation amplitude increases. Simultaneously, the thrust coefficient significantly increases, allowing the undulating fin to maintain effective operational performance even at larger amplitudes.

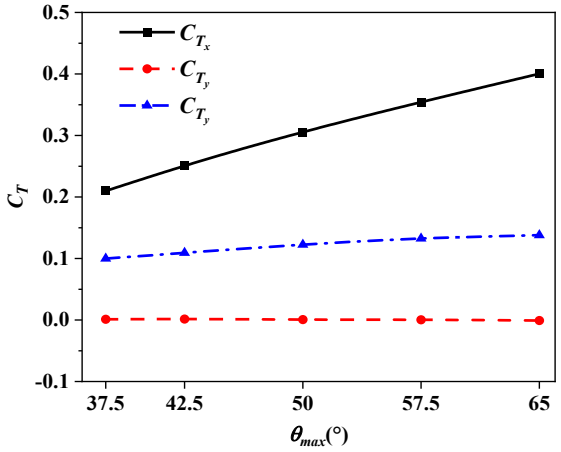

Fig. 12. Variation curves of force coefficients at different oscillation angles.

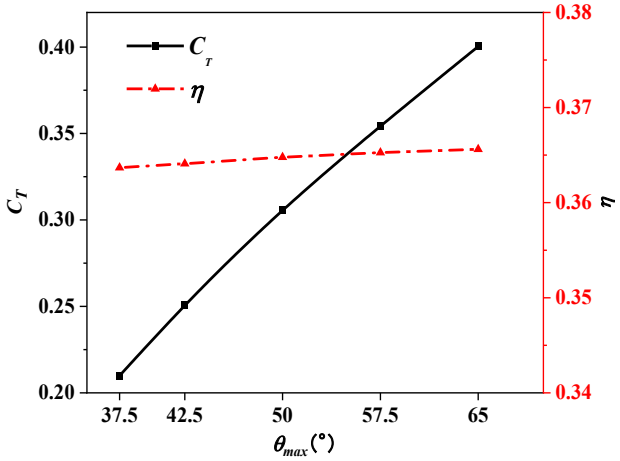

Fig. 13. Hydrodynamic characteristic curves at different angles of attack.

As illustrated in Figure 14, the vorticity contours of the undulating fin at varying amplitudes illustrate the formation of a typical reverse Kármán vortex street at the trailing edge, characterized by alternating vortices. The study reveals that as the amplitude increases, both the number and intensity of the vortices significantly increase. This suggests that larger amplitude generates stronger vortices, and the increase in oscillation amplitude exerts a positive and consistent influence on thrust, thereby confirming the previously mentioned variations in the thrust coefficient and enhancing the propulsion capability of the fins.

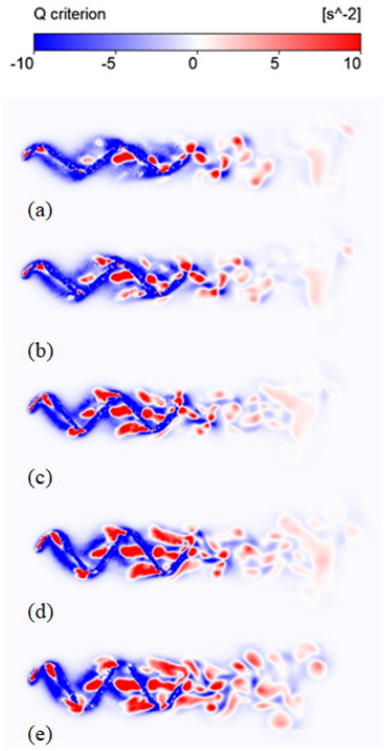

Fig. 14. Vorticity contour plots of the undulating fin under various amplitude conditions: (a) θ_{max}=37.5°, (b) θ_{max}=42.5°, (c) θ_{max}=50°, (d) θ_{max}=57.5°, (e) θ_{max}=65°.

4 Conclusion

To enhance the understanding of the propulsion performance of three-dimensional, large-amplitude undulating fins, this study presents several significant contributions. Using the knifefish (Apteronotus albifrons) as a biomimetic model, we design a novel large-amplitude torsional wave propulsion fin. The research employs dynamic grid techniques, including diffusion smoothing and local grid reconstruction models, to effectively capture the complex movements of the fin and their effects on hydrodynamic characteristics. This study simulates large-amplitude torsional wave propulsion with a maximum oscillation amplitude of ±65°. Additionally, it elucidates the impact of large amplitudes on the thrust and propulsion efficiency of the undulating fin. The primary research findings are presented as follows:

1. This paper examines the thrust and propulsion efficiency of an undulating fin, examining the effects of flow velocity and oscillation amplitude on its performance. The results indicate that as the advance ratio (i.e. the flow velocity) increases, the thrust coefficient gradually decreases, while the average propulsion efficiency initially increases before subsequently decreasing. When J= 0.75 (U_0 = 1 kn), θ_{max} = 50°,

and f = 1 Hz, the maximum average efficiency η reaches 68.5% in the calculated working conditions.

2. As the amplitude of the undulating fin's oscillation increases, the average propulsion efficiency of the undulating fin remains stable at approximately 36.5%, demonstrating consistent performance. Simultaneously, the thrust coefficient significantly increases, allowing the undulating fin to maintain effective operational performance even at larger amplitudes.

3. A more detailed analysis is conducted on the vorticity curves of the undulating fin under varying advance ratios and amplitude conditions. As the amplitude increases, both the quantity and intensity of the vortices significantly increase. Consequently, this enhancement increases the propulsion efficiency of the undulating fin.

This research further investigates the intricate interactions between large-amplitude undulating fins and fluid flow. However, due to simplifications in the model, certain limitations exist, as factors such as fin thickness and material properties are not fully addressed. This oversight may result in suboptimal flexibility and efficiency within the propulsion system. Future research should incorporate fin thickness, material properties, and fluid-structure interactions, along with multi-condition testing and experimental validation, to optimize biomimetic design and enhance the performance and practicality of the propulsion system.

References

1. Zeng X, Xia M, Luo Z, et al. Design and control of an underwater robot based on hybrid propulsion of quadrotor and bionic undulating fin[J]. Journal of Marine Science and Engineering, 2022, 10(9): 1327. https://doi.org/10.3390/jmse10091327.
2. Epstein M, Colgate J E and MacIver M A. A biologically inspired robotic ribbon fin[C]//Proceedings of the 2005 IEEE/RSJ International Conference on Intelligent Robots and Systems (IROS), workshop on Morphology, Control, and Passive Dynamics. 2005. https://doi.org/10.1109/IROS.2006.281681.
3. WANG Guang-ming. Theoretic and experimental research on propulsion by bionic undulatory fin[D]. Changsha, China: National University of Defense Technology, 2007.
4. Chang Wei, Qiao Hu, Shijie Li, Tangjia Zhang and Xindong Shi; Hydrodynamic performance analysis of undulating fin propulsion. Physics of Fluids 1 September 2023; 35 (9): 091906. https://doi.org/10.1063/5.0170156.
5. Liu L, Li Y, Wang Y, et al. Design and preliminary evaluation of a biomimetic underwater robot with undulating fin propulsion[C]//IOP Conference Series: Materials Science and Engineering. IOP Publishing, 2020, 790(1): 012160. https://doi.org/10.1088/1757-899X/790/1/012160.
6. Zhang M, Wang C and Su Y. Hydrodynamic characteristics of an electric eel-like undulating fin[J]. Journal of Applied Fluid Mechanics, 2023, 16(5): 1030-1043.
7. Liu F and Ji S. Unsteady flow calculations with a multigrid Navier-Stokes method[J]. AIAA journal, 1996, 34(10): 2047-2053. https://doi.org/10.2514/3.13351.
8. Wilcox D C. Reassessment of the scale-determining equation for advanced turbulence models[J]. AIAA journal, 1988, 26(11): 1299-1310. https://doi.org/10.2514/3.10041.

9. Maertens A P, Triantafyllou M S and Yue D K P. Efficiency of fish propulsion[J]. Bioinspiration & biomimetics, 2015, 10(4): 046013. https://doi.org/10.1088/1748-3190/10/4/046013.
10. Sun G, Wang Z, Ling H, et al. Investigation on the propulsive efficiency of undulating fin propulsor[J]. Ocean Engineering, 2024, 312: 119113. https://doi.org/10.1016/j.oceaneng.2024.119113.